Control of the absorption of a four-level quantum system near a plasmonic nanostructure

F. Carreño,[1] M. A. Antón,[1] V. Yannopapas,[2] and E. Paspalakis[3]
[1]*Facultad de Óptica y Optometría, Universidad Complutense de Madrid, Avenida Arcos de Jalón 118, 28037 Madrid, Spain*
[2]*Department of Physics, National Technical University of Athens, Athens 157 80, Greece*
[3]*Department of Materials Science, School of Natural Sciences, University of Patras, Patras 265 04, Greece*
(Received 2 December 2016; revised manuscript received 10 April 2017; published 11 May 2017)

We study the optical response of a four-level double-V-type quantum system which interacts simultaneously with probe and pump laser fields and is located near a two-dimensional array of metal-coated dielectric nanospheres. By considering different coupling configurations for the pump/probe laser fields and analyzing the resulting probe absorption spectrum we reveal a variety of phenomena, such as huge enhancement of the absorption at the central line, gain without inversion, and a phase-dependent absorption spectrum. We also show that the enhancement of probe absorption or the gain can be controlled by varying the distance of the quantum system from the plasmonic nanostructure, the intensity of the pump field(s), and, when applicable, their relative phase. Our results can find applications in on-chip nanoscale photonic devices.

DOI: 10.1103/PhysRevB.95.195410

I. INTRODUCTION

The strong interaction of light with quantum systems near plasmonic nanostructures leads to significantly modified (mainly enhanced) nonlinear optical phenomena at the nanoscale. These phenomena are attributed to three main factors: (a) the strong enhancement of the applied electric field, (b) the significant modification of the quantum system's spontaneous decay rate, and (c) the strong exciton-plasmon coupling occurring for quantum systems near plasmonic nanostructures. Some of the effects that have been studied in this research area are Fano effects in energy absorption [1–4], ultrafast switching and controlled population transfer [5–11], gain without inversion [12–15], quantum-coherence-enhanced surface-plasmon amplification [16], controlled optical bistability and multistability [17–20], strongly modified four-wave mixing [21–24], enhanced second-harmonic generation [25,26] and nonlinear optical rectification [27], single [28] and double [29] optical transparency accompanied by slow light, phase control of absorption and dispersion [30], strongly enhanced Kerr nonlinearity [31–34], and controlled Goos-Hänchen shift [35]. These phenomena have various potential applications in nanophotonics and in quantum technology at the nanoscale, such as in controllable in ultrafast nanoswitches, in ultrasensitive nanosensors, in enhancing the power generated by a photovoltaic device or the efficiency of a photodetector, in quantum information processing, and in on-chip nanoscale photonic nonlinear devices.

A quantum system that has shown remarkable optical response is a four-level double-V-type quantum system that exhibits quantum interference in spontaneous emission when placed near a two-dimensional array of metal-coated dielectric nanospheres. In this quantum system, one V-type transition is influenced by the interaction with localized surface plasmons, while the other V-type transition interacts with free-space vacuum and with the external laser fields. When this system interacts with a weak probe laser field, it leads to optical transparency accompanied with slow light [28] and strongly modified Kerr nonlinearity [31]. Additionally, when the system interacts with two weak fields it leads to phase-dependent complete optical transparency and gain without inversion [30].

Many times, in coupled quantum-plasmonic nanostructures, a strong pump laser field is used for the control of the optical properties of a weak probe laser field [12,14,15,21–23,29,32,34]. The combination of the pump field with the plasmonic nanostructure leads to a significantly modified optical response for the quantum system when compared with the case where the quantum system is located in free space. Here, we study the optical response of the four-level double-V-type quantum system near a two-dimensional array of metal-coated dielectric nanospheres when it interacts simultaneously with a weak probe laser field and with one or two moderate/strong pump laser fields. Both the quantum system and the plasmonic nanostructure are shown in Fig. 1. We consider different coupling configurations for the probe and pump fields that lead to different optical effects, such as huge enhancement of the absorption at the central line, gain without inversion, and a phase-dependent absorption spectrum. We also show that the enhancement of absorption or the gain can be controlled through different external parameters: the distance of the quantum system from the nanostructure, the intensity of the pump field(s) and, when applicable, their relative phase.

The article is organized as follows. In the next section we employ the density matrix equations for the description of the interaction of the quantum system with the laser fields under the influence of the plasmonic nanostructure and use it in order to calculate the absorption spectrum. Then, in Sec. III we present results for the absorption spectrum of the probe field under three different pump field couplings for various parameters of the system. In Sec. IV we summarize our findings. Finally, we present an Appendix with details of the calculation of the absorption spectrum.

II. THEORETICAL MODEL

The quantum system under study is shown in Fig. 1(c). We consider a four-level system with two closely lying upper states $|2\rangle$ and $|3\rangle$, and two lower states $|0\rangle$ and $|1\rangle$ such that the transition $|0\rangle \leftrightarrow |1\rangle$ is dipolar forbidden. We will call this system a double-V-type system in order to identify easily two different three-level V-type transitions in the structure. The

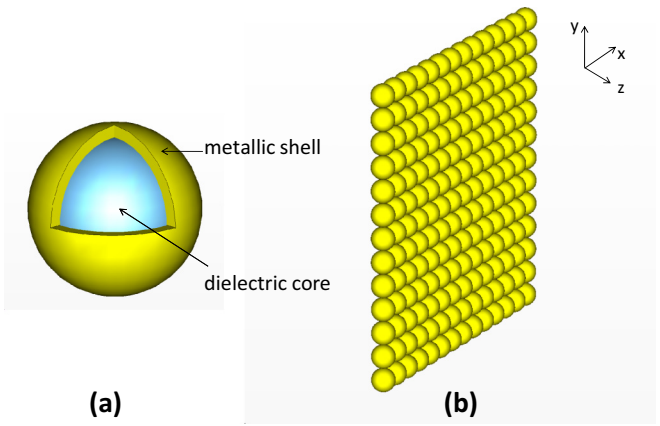

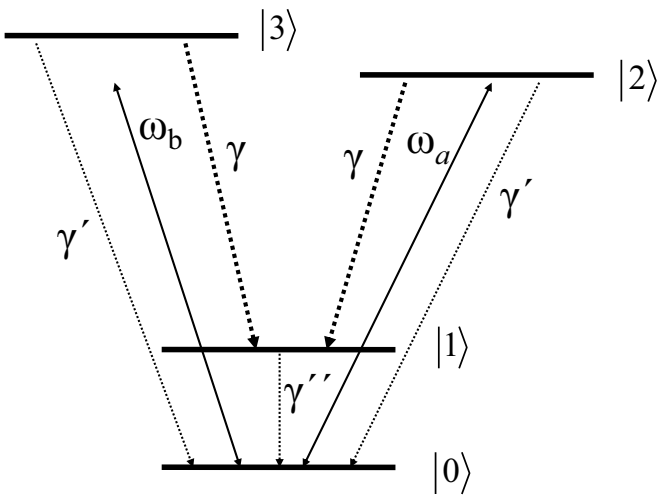

FIG. 1. (a) A metal-coated dielectric nanosphere and (b) a two-dimensional array of such spheres used in this work. (c) The energy-level diagram of the quantum system and the relevant couplings. The two upper states $|2\rangle$ and $|3\rangle$ decay with spontaneous emission to the two lower states $|0\rangle$ and $|1\rangle$. The transitions from $|0\rangle$ to $|2\rangle$ and $|3\rangle$ are driven by pump laser fields.

quantum system is located in vacuum at distance d from the surface of the plasmonic nanostructure, which is shown in Fig. 1(b). We take states $|2\rangle$ and $|3\rangle$ to characterize two Zeeman sublevels ($J = 1, M_J = \pm 1$), while the two lower states $|0\rangle$ and $|1\rangle$ are levels with $J = 0$. Then, the dipole moment operator is taken as

$$\vec{\mu} = \mu'(|2\rangle\langle 0|\hat{\varepsilon}_- + |3\rangle\langle 0|\hat{\varepsilon}_+) + \mu(|2\rangle\langle 1|\hat{\varepsilon}_- + |3\rangle\langle 1|\hat{\varepsilon}_+), \quad (1)$$

where $\hat{\varepsilon}_\pm = (\mathbf{e}_z \pm i\mathbf{e}_x)/\sqrt{2}$ describes the right-rotating ($\hat{\varepsilon}_+$) and left-rotating ($\hat{\varepsilon}_-$) unit vectors, and μ, μ' are taken to be real.

The Hamiltonian that governs the dynamics of the quantum system can be expressed as

$$H = H_s + H_{\text{ext}} + H_f + H_i. \quad (2)$$

The Hamiltonian of the system reads

$$H_s = \sum_{j=0}^{j=3} E_j \sigma_{jj}, \quad (3)$$

where $E_j = \hbar\omega_j$ is the energy of the jth state and $\sigma_{jj} = |j\rangle\langle j|$. We assume that the two upper levels are degenerated ($E_3 = E_2$).

The quantum system interacts in general with two circularly polarized continuous wave pump electromagnetic (laser) fields, with total electric field

$$\vec{\mathcal{E}}(t) = \hat{\varepsilon}_+ \mathcal{E}_a \cos(\omega_a t + \phi_a) + \hat{\varepsilon}_- \mathcal{E}_b \cos(\omega_b t + \phi_b), \quad (4)$$

where $\mathcal{E}_a$ ($\mathcal{E}_b$) is the electric field amplitude, ω_a (ω_b) is the angular frequency, and ϕ_a (ϕ_b) is the phase of field a (b). The pump field a couples state $|0\rangle$ with state $|2\rangle$, and the pump field b couples state $|0\rangle$ with state $|3\rangle$. We assume that both fields have equal frequencies $\omega_a = \omega_b = \omega_L$. The Hamiltonian that describes the interaction of the electromagnetic field with the quantum system, in the dipole and rotating wave approximations, is given by

$$H_{\text{ext}} = -\hbar\Omega_a e^{-i(\omega_L t + \phi_a)}\sigma_{20} - \hbar\Omega_b e^{-i(\omega_L t + \phi_b)}\sigma_{30} + \text{H.a.}, \quad (5)$$

where we have defined $\Omega_a = \mu'\mathcal{E}_a/\hbar$, $\Omega_b = \mu'\mathcal{E}_b/\hbar$, and H.a. stands for Hermitian adjoint.

We assume that the transitions $|2\rangle$, $|3\rangle$ to $|1\rangle$ lie within the surface-plasmon bands of the plasmonic nanostructure, whereas the transitions $|2\rangle$, $|3\rangle$ to $|0\rangle$ are spectrally distant from the surface-plasmon bands and are thus not influenced by the plasmonic nanostructure, as it was considered in Ref. [36]. Therefore, in the transitions $|2\rangle$, $|3\rangle$ to $|0\rangle$ the spontaneous decay occurs due to the interaction of the quantum system with free-space vacuum electromagnetic modes. In view of the previous considerations, the term H_f in Eq. (2) associated to the medium-assisted electromagnetic field is split as

$$H_f = H_{f,0} + H_{f,1}. \quad (6)$$

The free Hamiltonian describing the interaction with ordinary vacuum reads

$$H_{f,0} = \hbar \sum_{k,\lambda} \omega_{k\lambda} a^\dagger_{k\lambda} a_{k\lambda}, \quad (7)$$

$a_{k\lambda}$ being a set of bosonic operators obeying the usual commutation rules: $[a_{k\lambda}, a^\dagger_{k'\lambda'}] = \delta_{kk'}\delta_{\lambda\lambda'}$, and λ an index for polarization.

The free Hamiltonian describing the interaction with the plasmon-modified modes reads

$$H_{f,1} = \hbar \int d\vec{r} \int_0^\infty d\omega\, \omega\, \vec{f}^\dagger_\lambda(\vec{r},\omega)\vec{f}_\lambda(\vec{r},\omega), \quad (8)$$

which is given in terms of a set of bosonic fields $\vec{f}_\lambda(\vec{r},\omega)$. Here $\vec{f}_\lambda(\vec{r},\omega)$ plays the role of the variable of the electromagnetic field and the medium, including a reservoir associated to the losses in the medium. The field operators obey the usual commutation rules:

$$[\vec{f}_\lambda(\vec{r},\omega), \vec{f}^\dagger_{\lambda'}(\vec{r}',\omega')] = \delta_{\lambda\lambda'}\delta(\omega - \omega')\delta(\vec{r} - \vec{r}'). \quad (9)$$

The interaction Hamiltonian is split into two terms as

$$H_i = H_{i,0} + H_{i,1}. \tag{10}$$

The first term in Eq. (10) accounts for the interaction with ordinary vacuum and reads

$$H_{i,0} = \hbar \sum_{k,\lambda} (g_{02}^{-} a_{k\lambda}\sigma_{20} + g_{03}^{+} a_{k\lambda}\sigma_{30} + \text{H.a.}), \tag{11}$$

the parameter $g_{0k}^{\mp} = -\sqrt{\omega_{k\lambda}/2\hbar\epsilon_0 V}\,\mu' \hat{\varepsilon}_{\mp}\cdot\hat{e}_{k\lambda}$ being the coupling constant of the atomic transition $|m\rangle \leftrightarrow |0\rangle$ $(m = 2,3)$ with the electromagnetic mode.

The second term in Eq. (10) is for the interaction with plasmon-modified modes and reads

$$H_{i,1} = -\int_0^{\infty} d\omega[\vec{\mu}_1 \cdot \vec{E}(\vec{r},\omega) + \text{H.a.}], \tag{12}$$

where $\vec{\mu}_1 = \mu(|2\rangle\langle 1|\hat{\varepsilon}_- + |3\rangle\langle 1|\hat{\varepsilon}_+)$, and $\vec{E}(\vec{r},\omega)$ is the field operator (excluding the external driving field), which is defined through [37]

$$\vec{E}(\vec{r},\omega) = i\sqrt{\frac{\hbar}{\pi\epsilon_0}}\frac{\omega^2}{c^2}\int d\vec{r}\,'\sqrt{\epsilon_I(\vec{r}\,',\omega)}\overleftrightarrow{G}(\vec{r},\vec{r}\,',\omega)\vec{f}(\vec{r}\,',\omega), \tag{13}$$

where $\overleftrightarrow{G}(\vec{r},\vec{r}\,',\omega)$ is the dyadic Green's tensor. Here, $\epsilon(\vec{r}\,',\omega) = \epsilon_R(\vec{r}\,',\omega) + \epsilon_I(\vec{r}\,',\omega)$ stands for the complex permittivity.

We transform the Hamiltonian in Eq. (2) to the interaction picture using $\tilde{H} \to U^{\dagger}(t)HU(t)$, with $U(t) = \exp[-i(H_s + H_f)t]$, where the tilde denotes the interaction picture. Here it is worth mentioning that the system remains within the weak-coupling regime, as we will consider distances between the quantum system and the metallic nanostructure such that strong-coupling effects do not emerge (see Refs. [38–41] for details concerning the strong-coupling regime). We next manipulate the interaction of the system with the two reservoirs to derive a master equation within the Born-Markov approximation for the reduced density operator ρ_s by carrying out the trace over the baths' operators while assuming the zero-temperature bath limit for both reservoirs, and moving back to the Schrödinger picture. The resulting master equation reads

$$\frac{\partial\rho_s}{\partial t} = -\frac{i}{\hbar}[H_e,\rho_s] + \mathcal{L}\rho_s, \tag{14}$$

where $H_e = H_A + H_{\text{ext}}$ stands for the atomic plus coherent part of the Hamiltonian which in an appropriate rotating frame reduces to

$$H_e = -\hbar\delta(\sigma_{22}+\sigma_{33}) - \left(\frac{\hbar\Omega_a e^{i\phi}}{2}\sigma_{02} + \frac{\hbar\Omega_b}{2}\sigma_{03} + \text{H.a.}\right). \tag{15}$$

Here, $\delta = \omega_L - \tilde{\omega}$ is the detuning from resonance with the average transition energies of states $|2\rangle$ and $|3\rangle$ from state $|0\rangle$, with $\tilde{\omega} = (\omega_3+\omega_2)/2 - \omega_0$, and $\phi = \phi_a - \phi_b$ is the phase difference of the two pump fields. We remind here that we have assumed the system to be degenerate $\omega_{32} = \omega_3 - \omega_2 = 0$.

The operator $\mathcal{L}\rho_s$ in Eq. (14) accounts for the dissipation processes which in the Linblad form reads as

$$\begin{aligned}\mathcal{L}\rho_s = &+\gamma'(2\sigma_{02}\rho_s\sigma_{20} - \sigma_{22}\rho_s - \rho_s\sigma_{22})\\ &+\gamma'(2\sigma_{03}\rho_s\sigma_{30} - \sigma_{33}\rho_s - \rho_s\sigma_{33})\\ &+\gamma(2\sigma_{12}\rho_s\sigma_{21} - \sigma_{22}\rho_s - \rho_s\sigma_{22})\\ &+\gamma(2\sigma_{13}\rho_s\sigma_{31} - \sigma_{33}\rho_s - \rho_s\sigma_{33})\\ &+\kappa(2\sigma_{13}\rho_s\sigma_{21} - \sigma_{23}\rho_s - \rho_s\sigma_{23})\\ &+\kappa(2\sigma_{12}\rho_s\sigma_{31} - \sigma_{32}\rho_s - \rho_s\sigma_{32})\\ &+\gamma''(2\sigma_{01}\rho_s\sigma_{10} - \sigma_{11}\rho_s - \rho_s\sigma_{11}).\end{aligned} \tag{16}$$

The two first terms in Eq. (16) involve magnitude γ' ($\gamma' = \mu'^2\bar{\omega}^3/(3\pi\epsilon_0\hbar c^3)$ corresponds to the decay rate of an atomic transition in free space). In the current scheme the decay from the two upper states to the lower level is the same. The term involving γ'' arises from a dipolar forbidden transition, and thus we expect that $\gamma'' \ll \gamma,\gamma'$.

The values of γ and κ are obtained by [42–45]

$$\begin{aligned}\gamma &= \frac{\mu_0\mu^2\bar{\omega}^2}{\hbar}\hat{\varepsilon}_-\cdot\text{Im}\mathbf{G}(\mathbf{r},\mathbf{r};\bar{\omega})\cdot\hat{\varepsilon}_+\\ &= \frac{\mu_0\mu^2\bar{\omega}^2}{2\hbar}\text{Im}[G_{\perp}(\mathbf{r},\mathbf{r};\bar{\omega}) + G_{\parallel}(\mathbf{r},\mathbf{r};\bar{\omega})]\\ &= \frac{1}{2}(\Gamma_{\perp}+\Gamma_{\parallel}),\end{aligned} \tag{17}$$

$$\begin{aligned}\kappa &= \frac{\mu_0\mu^2\bar{\omega}^2}{\hbar}\hat{\varepsilon}_+\cdot\text{Im}\mathbf{G}(\mathbf{r},\mathbf{r};\bar{\omega})\cdot\hat{\varepsilon}_+\\ &= \frac{\mu_0\mu^2\bar{\omega}^2}{2\hbar}\text{Im}[G_{\perp}(\mathbf{r},\mathbf{r};\bar{\omega}) - G_{\parallel}(\mathbf{r},\mathbf{r};\bar{\omega})]\\ &= \frac{1}{2}(\Gamma_{\perp}-\Gamma_{\parallel}).\end{aligned} \tag{18}$$

Here, κ is the coupling coefficient between states $|2\rangle$ and $|3\rangle$ due to the anisotropic Purcell effect [46], which is responsible for the appearance of quantum interference in spontaneous emission [36,42–45,47–49]. $\mathbf{G}(\mathbf{r},\mathbf{r};\omega)$ stands for the dyadic electromagnetic Green's tensor, where $\mathbf{r}$ refers to the position of the quantum system, and μ_0 is the permeability of vacuum. In addition, $G_{\perp}(\mathbf{r},\mathbf{r};\bar{\omega}) = G_{zz}(\mathbf{r},\mathbf{r};\bar{\omega})$, $G_{\parallel}(\mathbf{r},\mathbf{r};\bar{\omega}) = G_{xx}(\mathbf{r},\mathbf{r};\bar{\omega})$ denote the components of the electromagnetic Green's tensor where the symbol $\perp$ ($\parallel$) refers to a dipole-oriented normal, along the z axis (parallel, along the x axis) to the surface of the nanostructure. Finally, we define the spontaneous emission rates normal and parallel to the surface as $\Gamma_{\perp,\parallel} = \mu_0\mu^2\bar{\omega}^2\text{Im}[G_{\perp,\parallel}(\mathbf{r},\mathbf{r};\bar{\omega})]/\hbar$. The degree of quantum interference is defined as

$$p = (\Gamma_{\perp}-\Gamma_{\parallel})/(\Gamma_{\perp}+\Gamma_{\parallel}). \tag{19}$$

For $p = 1$ we have maximum quantum interference in spontaneous emission [48]. This can be achieved by placing the quantum system close to a photonic structure that completely quenches $\Gamma_{\parallel}$. We stress that when the quantum system is placed in vacuum, $\Gamma_{\perp} = \Gamma_{\parallel}$ and $\kappa = 0$, so no quantum interference occurs in the system.

The plasmonic nanostructure considered in this study is a two-dimensional array of touching metal-coated silica nanospheres [see Figs. 1(a) and 1(b)]. The dielectric function

of the shell is provided by a Drude-type electric permittivity given by

$$\epsilon(\omega) = 1 - \frac{\omega_p^2}{\omega(\omega + i/\tau)}, \tag{20}$$

where ω_p is the bulk plasma frequency and τ the relaxation time of the conduction-band electrons of the metal.

The electromagnetic Green's tensor that provides $\Gamma_\perp$, $\Gamma_\parallel$ is given by [47,50,51]

$$G_{ii'}^{EE}(\mathbf{r},\mathbf{r}';\omega) = g_{ii'}^{EE}(\mathbf{r},\mathbf{r}';\omega) - \frac{i}{8\pi^2}\int\int_{\mathrm{SBZ}} d^2\mathbf{k}_\parallel \sum_{\mathbf{g}} \frac{1}{c^2 K_{\mathbf{g};z}^+} \times v_{\mathbf{g}\mathbf{k}_\parallel;i}(\mathbf{r}) \exp(-i\mathbf{K}_\mathbf{g}^+ \cdot \mathbf{r})\hat{\mathbf{e}}_{i'}(\mathbf{K}_\mathbf{g}^+), \tag{21}$$

with

$$v_{\mathbf{g}\mathbf{k}_\parallel;i}(\mathbf{r}) = \sum_{\mathbf{g}'} R_{\mathbf{g}';\mathbf{g}}(\omega,\mathbf{k}_\parallel)\exp(-i\mathbf{K}_{\mathbf{g}'}^- \cdot \mathbf{r})\hat{\mathbf{e}}_i(\mathbf{K}_{\mathbf{g}'}^-) \tag{22}$$

and

$$\mathbf{K}_\mathbf{g}^\pm = (\mathbf{k}_\parallel + \mathbf{g}, \ \pm[q^2 - (\mathbf{k}_\parallel + \mathbf{g})^2]^{1/2}). \tag{23}$$

The vectors $\mathbf{g}$ denote the reciprocal-lattice vectors corresponding to the 2D periodic lattice of the plane of scatterers and $\mathbf{k}_\parallel$ is the reduced wave vector which lies within the surface Brillouin zone associated with the reciprocal lattice [52]. When $q^2 = \omega^2/c^2 < (\mathbf{k}_\parallel + \mathbf{g})^2$, $\mathbf{K}_\mathbf{g}^\pm$ defines an evanescent wave. The term $g_{ii'}^{EE}(\mathbf{r},\mathbf{r}';\omega)$ of Eq. (21) is the free-space Green's tensor and $\hat{\mathbf{e}}_i(\mathbf{K}_\mathbf{g}^\pm)$ the polar unit vector normal to $\mathbf{K}_\mathbf{g}^\pm$. $R_{\mathbf{g}';\mathbf{g}}(\omega,\mathbf{k}_\parallel)$ is the reflection matrix, which provides the sum (over $\mathbf{g}$'s) of reflected beams generated by the incidence of plane wave from the left of the plane of scatterers [52]. Also, in Eq. (21), the terms corresponding to s-polarized waves (those containing components with the azimuthal unit vector $\hat{\mathbf{e}}_i(\mathbf{K}_\mathbf{g}^\pm)$ normal to $\mathbf{K}_\mathbf{g}^\pm$) have small contribution to the decay rates and have been, therefore, neglected.

The equations for the density matrix elements of the system are derived from Eq. (14) (see Appendix). We are interested in the spectral absorption of a weak probe laser field with angular frequency ω_p which scans along either one or the two free-space transitions $|0\rangle \leftrightarrow |2\rangle$ and $|0\rangle \leftrightarrow |3\rangle$, while the system is driven by moderate to strong pump laser field(s) along the same transitions. In the steady-state regime, the absorption spectrum is proportional to the Fourier transformation of the correlation function $\lim_{t\to\infty}\langle[\vec{E}^-(r,t'+t),\vec{E}^+(r,t)]\rangle$, where $\vec{E}^-(r,t)/\vec{E}^+(r,t)$ is the negative/positive frequency part of the radiation field in the far zone. The radiation field consists of a free-field operator and a source-field operator that is proportional to the atomic polarization operator [53]. Therefore, the steady-state absorption spectrum can be expressed in terms of the atomic correlation function

$$A(\omega) = \mathrm{Re}\left(\lim_{t\to\infty}\int_0^\infty \langle[\vec{E}^-(t'+t),\vec{E}^+(t)]\rangle e^{-i\omega t'}dt'\right), \tag{24}$$

where Re( ) denotes the real part of the magnitude enclosed in parenthesis. Also, $\vec{E}^+(t)$ is the positive frequency part of the fluorescent field, which in the far-field zone ($|\vec{r}| \gg c/\omega_{j0}$, $j = 2,3$) reads

$$\vec{E}^+(\vec{r},t) = \frac{\omega_{30}^2}{c^2|\vec{r}|}\vec{\mu}_{03}\sigma_{30}(t - |\vec{r}|/c) + \frac{\omega_{20}^2}{c^2|\vec{r}|}\vec{\mu}_{02}\sigma_{20}(t - |\vec{r}|/c), \tag{25}$$

and $\vec{E}^-(t) = (\vec{E}^+(t))^\dagger$. We will assume that $\omega_{30} = \omega_{20}$. Substituting Eq. (25) into Eq. (24) results in an expression containing two-time correlation functions which are determined by invoking of the quantum regression theorem [53,54] (see Appendix for details). The absorption spectrum given by Eq. (24) has two contributions: one of them accounts for the photons absorbed along the $|0\rangle \leftrightarrow |3\rangle$ transition [the terms involving $\hat{U}_{03}(\tau)$ and $\hat{U}_{30}(\tau)$ as defined in Appendix], while the other is related with the photons absorbed along the $|0\rangle \leftrightarrow |2\rangle$ path [the terms involving $\hat{U}_{02}(\tau)$ and $\hat{U}_{20}(\tau)$]. In writing Eq. (24) and in what follows, we abbreviate $\omega_p - \omega_L$ by ω, but we should interpret ω as a frequency measured relative to the laser frequency ω_L, since we will assume that the hybrid system is driven by a single or two pump laser fields.

III. NUMERICAL RESULTS

We will study the absorption spectrum of a weak probe laser field under different coupling configurations of the pump laser fields. We assume the following parameters for the elements of the metallic nanostructure: the dielectric constant of SiO_2 is taken to be $\epsilon = 2.1$. In the calculations we have taken $\tau^{-1} = 0.05\omega_p$, ω_p being the plasma frequency for gold taken as $\hbar\omega_p = 8.99$ eV [55], which in turn determines the length scale of the system as $c/\omega_p \approx 22$ nm. The lattice constant of the square lattice is $a = 2c/\omega_p$ and the sphere radius $S = a/2 = c/\omega_p$ with core radius $S_c = 0.7c/\omega_p$. We also take $\bar{\omega} = 0.632\omega_p$ and calculate the decay rates $\Gamma_\perp$ and $\Gamma_\parallel$ in the presence of the plasmonic nanostructure. The decay rates of the transitions are taken as $\gamma' = 0.3\Gamma_0$, $\gamma = (\Gamma_\parallel + \Gamma_\perp)/2$, and $\gamma'' = 0.001\Gamma_0$.

The results of the calculation of the decay rates are shown in Figs. 2(a) and 2(b). The large difference between $\Gamma_\perp$ and $\Gamma_\parallel$ due to the anisotropic Purcell effect is obvious. In addition, Fig. 2(c) displays the result for the quantum interference p computed using Eq. (19) versus the normalized distance. There we can see that (i) there is a nonmonotonic behavior of p on distance and (ii) the value of the quantum interference parameter remains high or very high ($p > 0.95$) in the range of distances considered.

A. Pumping one transition and probing the adjacent transition

First we assume that the pump field is applied on resonance only along the $|0\rangle \leftrightarrow |2\rangle$ transition ($\Omega_a \neq 0, \Omega_b = 0$, and $\delta = 0$). In addition, we consider that the weak probe field is applied along the $|0\rangle \leftrightarrow |3\rangle$ transition. Before presenting results for the absorption spectrum we analyze how the population is redistributed along the different states of the system under the application of the pump field. By solving Eq. (A11) we obtain the steady-state populations as a function of the Rabi frequency Ω_a, which are depicted in Fig. 3. We have selected distances where the effect of the plasmonic nanostructure is quite different. For the two shortest distances considered in

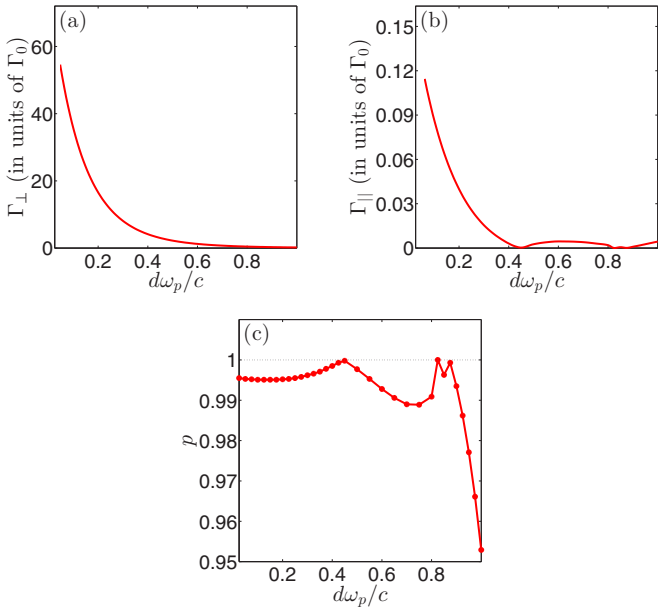

FIG. 2. (a)[(b)] The decay rates $\Gamma_\perp$ [$\Gamma_\parallel$] (in units of Γ_0, with Γ_0 being the decay rate in free space) versus the normalized distance $d\omega_p/c$ from the atomic system to the plasmonic nanostructure. (c) Quantum interference parameter p as defined in Eq. (19) versus the normalized distance $d\omega_p/c$.

Figs. 3(a) and 3(b), one of the decay rates is strongly enhanced with regard to the free-space value Γ_0, resulting in a strong acceleration of the decay to level $|1\rangle$. As for the third case considered in Fig. 3(c), the effect of the nanostructure is to slow down both decay rates [see Figs. 2(a) and 2(b)]. It is worth noting that, although the transition $|0\rangle \leftrightarrow |3\rangle$ is not driven by

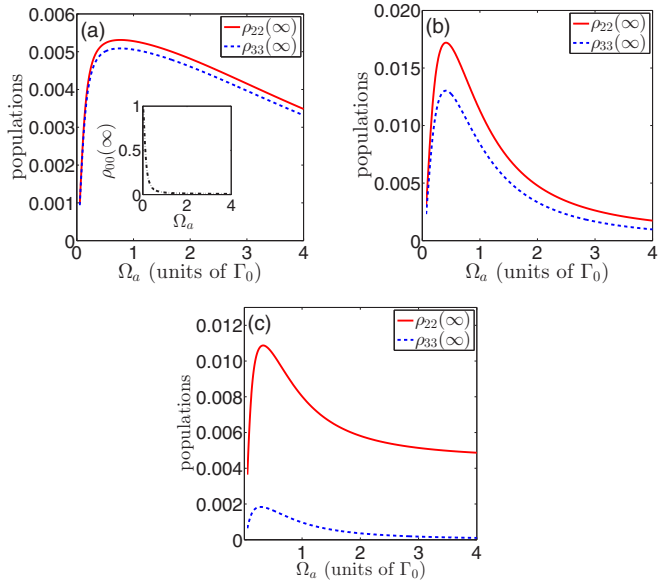

FIG. 3. Steady-state population of the states $|2\rangle$ (solid curve) and $|3\rangle$ (dashed curve) versus the Rabi frequency Ω_a for $\delta = 0$ for the following cases: (a) $d = 0.1c/\omega_p$, (b) $d = 0.4c/\omega_p$, and (c) $d = 0.8c/\omega_p$. The parameters used are $\Omega_b = 0$, $\delta = 0$, $\omega_{32} = 0$, $\gamma' = 0.3\Gamma_0$, and $\gamma'' = 0.001\Gamma_0$.

the pump laser field, a non-null value of the population of level $|3\rangle$ is obtained, which results from the quantum interference induced by the presence of the plasmonic nanostructure. In addition, we find the existence of an optimum Rabi frequency value ($\Omega_{a,\mathrm{opt}}$) which maximizes the steady-state population of the upper levels. For the shortest distance the value is $\Omega_{a,\mathrm{opt}} = 0.77\Gamma_0$; for the intermediate distance $\Omega_{a,\mathrm{opt}} = 0.41\Gamma_0$, while for the largest distance the Rabi frequency which maximizes population in level $|3\rangle$ is $\Omega^{(1)}_{a,\mathrm{opt}} = 0.29\Gamma_0$, whereas the one which maximizes population in level $|2\rangle$ is $\Omega^{(2)}_{a,\mathrm{opt}} = 0.33\Gamma_0$. In all cases we have checked that the following inequalities hold: $\rho_{22}(\infty) - \rho_{00}(\infty) < 0$ and $\rho_{33}(\infty) - \rho_{00}(\infty) < 0$, i.e., no inversion is achieved along the driven and the undriven channels in the bare basis. In addition, the population of the upper levels tends to become close to each other in the strong driving regime.

We want to point out that the role of the dissipative process along the channel $|0\rangle \leftrightarrow |1\rangle$ is essential to obtain a non-null probe absorption in steady state. Note that if we set $\gamma'' = 0$, and after a few cycles of the driving field, all population will be transferred to level $|1\rangle$ and the system will become completely transparent to the probe field in steady-state conditions. This relaxation along the dipolar forbidden transition $|0\rangle \leftrightarrow |1\rangle$ is therefore essential to the phenomenon we are considering, since it allows one to obtain a non-null value of population in the upper states at steady state. This kind of relaxation was also assumed in Ref. [56], where the quenching of spontaneous emission of an atomic system similar to the one we are considering was addressed.

We now proceed with the calculation of the probe absorption spectrum, based on Eq. (24). The corresponding results are depicted in Fig. 4 for different Rabi frequencies and distances of the quantum system from the plasmonic nanostructure. Note that in the absence of the nanostructure (not shown here), we obtain only a broad absorption line for the chosen values of the Rabi frequency of the pump field, since in that case level $|3\rangle$ remains unpopulated and the Autler-Townes splitting effect, that may occur here, is not prominent at these Rabi frequencies. Therefore, absorption at the central line is expected to be obtained due to the remaining population in level $|0\rangle$. However, the presence of the plasmonic nanostructure strongly modifies the absorption of the probe field. In Fig. 4(a) we present the results for the shortest distance, at three different Rabi frequencies. Here, the most interesting result relies on the creation of an extremely sharp dip in the absorption line in the range where $\Omega_a < \Gamma_0$; the dip disappears at large values of the Rabi frequency [see dashed-dotted line in Fig. 4(a)], and a small level of gain (without inversion) emerges close to the central line. The central dip changes to a huge absorption peak when the distance is increased up to $d = 0.4c/\omega_p$ as depicted in Fig. 4(b), which is more prominent in the regime of low pump fields. To better highlight the behavior of absorption at the central line, we present its value at $\omega = 0$ versus the distance d in Fig. 4(c). We have estimated that the absorption at the central line can be reduced to up to half of the value in free space for $d = 0.1c/\omega_p$ and can be enhanced up to a factor of 11 when $d = 0.4c/\omega_p$.

The previous findings can be attributed to the effect of quantum interference in the system which, although it takes

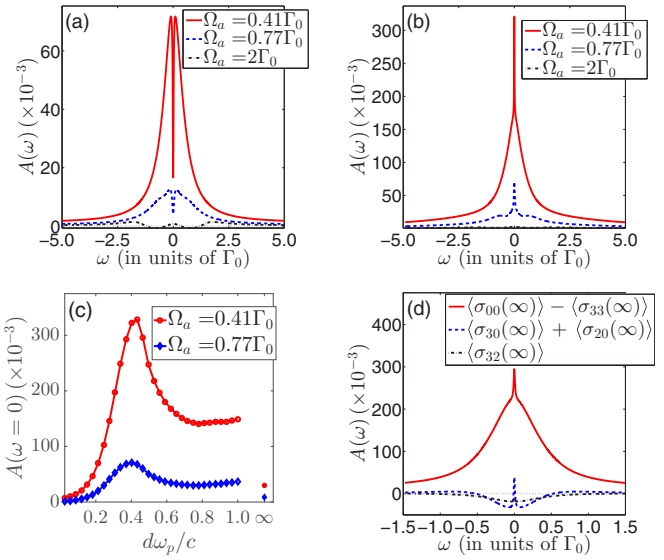

FIG. 4. Steady-state absorption spectrum $A(\omega)$ for the degenerate quantum system ($\omega_{32} = 0$) driven on resonance $\delta = 0$ along the transition $|0\rangle \leftrightarrow |2\rangle$ and probed along the transition $|0\rangle \leftrightarrow |3\rangle$ for distances: (a) $d = 0.1c/\omega_p$ and (b) $d = 0.4c/\omega_p$. The Rabi frequency of the pump field is set to $\Omega_a = 0.41\Gamma_0$ (solid curves), $\Omega_a = 0.77\Gamma_0$ (dashed curves), and $\Omega_a = 2\Gamma_0$ (dashed-dotted curves). (c) Steady-state absorption spectrum evaluated at the central line [$A(\omega = 0)$] versus the distance d for two Rabi frequencies: $\Omega_a = 0.41\Gamma_0$ ($\circ$) and $\Omega_a = 0.77\Gamma_0$ ($\diamond$). The filled symbols are obtained for $d = \infty$. (d) The various contributions to the absorption spectrum for $d = 0.4c/\omega_p$ and $\Omega_a = 0.41\Gamma_0$: the term proportional to $(\langle\sigma_{00}(\infty)\rangle - \langle\sigma_{33}(\infty)\rangle)$ (solid curve), the term proportional to $\langle\sigma_{30}(\infty)\rangle$ plus the one proportional to $\langle\sigma_{20}(\infty)\rangle$ (dashed curve), and the term proportional to $\langle\sigma_{32}(\infty)\rangle$ (dashed-dotted curve).

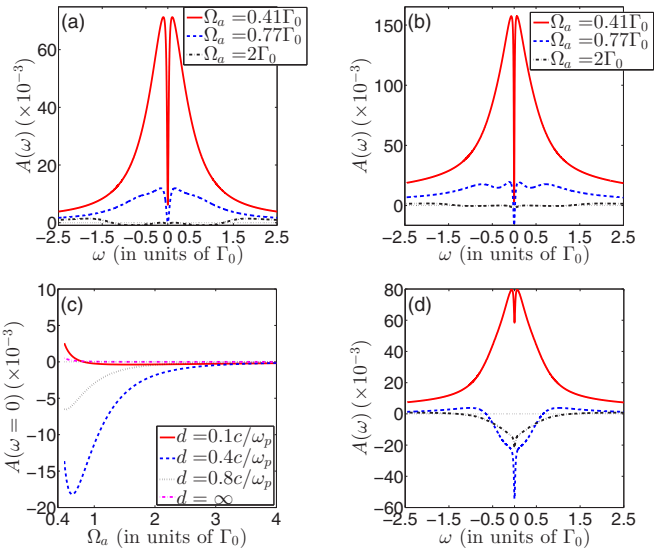

FIG. 5. Steady-state absorption spectrum $A(\omega)$ for the degenerate quantum system ($\omega_{32} = 0$) driven on resonance $\delta = 0$ along the transition $|0\rangle \leftrightarrow |2\rangle$ and probed along the transition $|0\rangle \leftrightarrow |2\rangle$ for distances: (a) $d = 0.1c/\omega_p$ and (b) $d = 0.4c/\omega_p$. The Rabi frequency of the driving field is set to $\Omega_a = 0.41\Gamma_0$ (solid curves), $\Omega_a = 0.77\Gamma_0$ (dashed curves), and $\Omega_a = 2\Gamma_0$ (dashed-dotted curves). The rest of the parameters are as in Figs. 4(a) and 4(b). (c) Steady-state absorption spectrum evaluated at the central line [$A(\omega = 0)$] versus the Rabi frequency for various distances: $d = 0.1c/\omega_p$ (solid curve), $d = 0.4c/\omega_p$ (dashed curve), $d = 0.8c/\omega_p$ (dotted curve), and $d = \infty$ (dashed-dotted curve). (d) Contributions to the absorption spectrum for $d = 0.4c/\omega_p$ and $\Omega_a = 0.63\Gamma_0$: the term proportional to $(\langle\sigma_{00}(\infty)\rangle - \langle\sigma_{33}(\infty)\rangle)$ (solid curve), the term proportional to $\langle\sigma_{30}(\infty)\rangle$ plus the one proportional to $\langle\sigma_{20}(\infty)\rangle$ (dashed curve), and the term proportional to $\langle\sigma_{23}(\infty)\rangle$ (dashed-dotted curve).

place along the undriven paths $|3\rangle \leftrightarrow |1\rangle$ and $|2\rangle \leftrightarrow |1\rangle$, it also modifies the probe field along the undriven and free-space decay path $|3\rangle \leftrightarrow |0\rangle$. Using Eq. (A17) in the Appendix, we can write the absorption spectrum for this particular case as

$$A(\omega) = R_{4,4}(\omega)(\langle\sigma_{00}(\infty)\rangle - \langle\sigma_{33}(\infty)\rangle) + R_{4,3}(\omega)\langle\sigma_{30}(\infty)\rangle + R_{4,8}(\omega)\langle\sigma_{20}(\infty)\rangle - R_{4,6}(\omega)\langle\sigma_{32}(\infty)\rangle. \quad (26)$$

Equation (26) indicates that the absorption spectrum has four different contributions: one proportional to the inversion of the probed transition (the first term which is proportional to $R_{4,4}$), the second and third terms are related with the steady-state value of the lower-to-upper-states coherences (proportional to $R_{4,3}$ and $R_{4,8}$), and the fourth term involves the upper-states coherence (proportional to $R_{4,6}$). In the absence of the plasmonic nanostructure, the second and fourth terms are null, whereas the first term dominates over the third term and results in the absorption of the weak probe. In the presence of the nanostructure, we have plotted apart in Fig. 4(d) the different contributions for the case exhibiting the largest enhancement of absorption at the central line (by selecting $d = 0.4c/\omega_p$, and $\Omega_a = 0.41\Gamma_0$). The solid curve is the one associated with the inversion and it always has a positive contribution to the spectrum. It consists of an extremely narrow Lorentzian line superimposed over a broad Lorentzian line. The ultranarrow feature is a signature of the emergence of quantum interference. The net contribution of the two terms related with the lower- and upper-level coherences, i.e., the dashed curve, also displays a narrow feature at the central line. Finally, the term involving the coherence of the upper states (dashed-dotted curve) has a negative sign but its effect is mostly overshadowed by the other terms.

B. Pumping and probing the same transition

We now consider that both the pump and the probe laser fields are applied along the $|0\rangle \leftrightarrow |2\rangle$ transition. The pump field is applied at exact resonance with the $|0\rangle \leftrightarrow |2\rangle$ transition ($\Omega_a \neq 0$, $\Omega_b = 0$, and $\delta = 0$). The results obtained for the absorption spectrum are depicted in Fig. 5(a)[(b)] when the distance is set to $d = 0.1c/\omega_p[d = 0.4c/\omega_p]$, for several Rabi frequencies. Here, we obtain the emergence of a hole burned into the central line also appearing in the absence of the nanostructure. For $d = \infty$ (absence of the plasmonic nanostructure) and at high enough Rabi frequencies, the system renders the probe almost transparent at $\omega = 0$; however $A(\omega) > 0$ for the whole spectral range (not shown here). However, the plasmonic nanostructure promotes the amplification of the probe field, as it is evidenced by the presence of gain at the central line. The level of gain is found to be dependent on both the distance d and the Rabi

frequency of the pump field. This is more clearly shown in Fig. 5(c), where we plot $A(\omega = 0)$ versus the Rabi frequency for several values of d. Namely, we find the existence of an optimum pump Rabi frequency which maximizes the gain at line center, which, for example, for $d = 0.4c/\omega_p$ assumes the value $\Omega_{a,\mathrm{opt}} = 0.63\Gamma_0$. The creation of gain at the line center can be understood as follows: most of the population is transferred to the long-lived state $|1\rangle$ by the pumping field, allowing the probe field to interact only with the nearly vanishing but non-null populations remaining in levels $|0\rangle$ and $|2\rangle$ (see Fig. 3). It is worth noting that gain is obtained without inversion in the bare basis.

We can get further insight about the origin of gain at the line center by using Eq. (A17) of the Appendix. In the current situation the absorption spectrum is determined through

$$A(\omega) = R_{6,6}(\omega)(\langle\sigma_{00}(\infty)\rangle - \langle\sigma_{22}(\infty)\rangle) + R_{6,9}(\omega)\langle\sigma_{30}(\infty)\rangle + R_{6,2}(\omega)\langle\sigma_{20}(\infty)\rangle - R_{6,4}(\omega)\langle\sigma_{23}(\infty)\rangle\,, \quad (27)$$

which indicates that the absorption spectrum has four different contributions: one proportional to the inversion of the probed transition (the first term which is proportional to $R_{6,6}$), the second and third terms which are related with the steady-state value of the lower-to-upper-states coherences (proportional to $R_{6,9}$ and $R_{6,2}$), and the fourth term which involves the upper-states coherence (proportional to $R_{6,4}$). In the absence of the plasmonic nanostructure the second and fourth terms are null, whereas the first term slightly dominates over the third term and results in weak probe absorption at line center, which is eventually reduced for large pump fields. In the case with the plasmonic nanostructure, we have plotted separately in Fig. 5(d) the different contributions for the case which exhibits the largest gain at $\omega = 0$ (by selecting $d = 0.4c/\omega_p$, and $\Omega_a = 0.63\Gamma_0$). The solid curve is the one associated with the population inversion and, as such, it always has a positive contribution to the spectrum; it consists of an extremely narrow dip superimposed over a broad Lorentzian line. The net contributions of the two terms related to the lower- and upper-level coherences (dashed curve) display also a narrow feature at the central line but of opposite sign relative to the previously mentioned term. Finally, the term involving the coherence of the upper states (dashed-dotted curve), whose ultimate origin relies upon the existence of quantum interference, has a negative sign and, as such, it is responsible for the existence of net gain.

C. Pumping and probing both transitions

In the last case we assume that the pump fields are applied along both transitions, field ω_a along the $|0\rangle \leftrightarrow |2\rangle$ transition and field ω_b along the $|0\rangle \leftrightarrow |3\rangle$ transition, with Rabi frequencies $\Omega_a = \Omega_b$, on resonance $\delta = 0$. In addition, we assume that the weak probe field is linearly polarized along the z axis, so that it can probe both transitions $|0\rangle \leftrightarrow |2\rangle$ and $|0\rangle \leftrightarrow |3\rangle$. In this case we expect the phase difference ϕ between the two pump laser fields to play an important role. As in the previous configurations, we first analyze how the population is distributed among states at steady state by solving Eq. (A11). The results for the upper-state populations are displayed in Fig. 6 for several distances between the quantum system and the nanostructure and different values

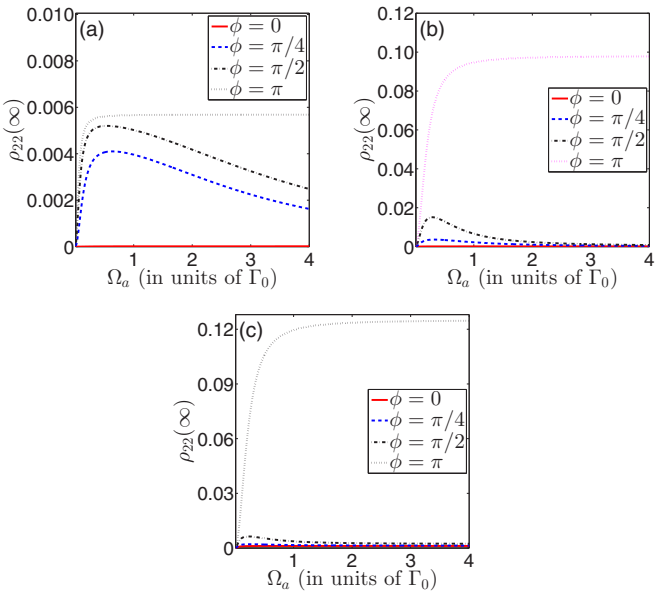

FIG. 6. Steady-state population of the state $|2\rangle$ versus the Rabi frequency Ω_a for different values of the phase difference: $\phi = 0$ (solid curve), $\phi = \pi/4$ (dashed curve), $\phi = \pi/2$ (dashed-dotted curve), and $\phi = \pi$ (dotted curve). The selected distances are (a) $d = 0.1c/\omega_p$, (b) $d = 0.4c/\omega_p$, and (c) $d = 0.8c/\omega_p$. We take $\Omega_b = \Omega_a$, while the rest of parameters are as in Fig. 3.

of ϕ. Note that due to the symmetry of the driven system, the upper levels are equally populated at steady state, i.e., $\rho_{22}(\infty) = \rho_{33}(\infty)$. From Fig. 6 we obtain that when both pump laser fields are in phase the population achieved at the upper levels is extremely small, whereas for values such as $\phi = \pi/4$ or $\phi = \pi/2$, an optimum Rabi frequency exists which maximizes the population of the upper levels. For $\phi = \pi$, the population transferred to the upper levels assumes its maximum values. The same holds for all distances, and the population asymptotically reaches a constant value for $\Omega > \gamma$.

We have found that the distribution of populations among the states of the system is highly sensitive to the phase difference ϕ and the Rabi frequency of the pump fields. This is also manifested in the absorption spectrum of the weak probe field. We note that recently, Pirruccio *et al.* observed a phase-dependent optical absorption for molecules near a metallic nanostructure [57]. The strong phase dependence in the probe absorption spectrum in our case is clearly shown in Figs. 7(a) and 7(b), for two Rabi frequencies and different values of ϕ, for the shortest distance of the quantum system from the nanostructure ($d = 0.1c/\omega_p$). We also plot the spectrum obtained for an isolated quantum system (thin solid curve). For $\Omega_a = 0.64\Gamma_0$, i.e., the Rabi frequency maximizing the population in the upper states [see Fig. 6(a)], we can see that the dip at the central line is highly narrowed. At the same time the peak value at the central line is either enhanced by a factor of 61 ($\phi = 0$) or reduced by a factor of 10 ($\phi = \pi$) in comparison with the isolated quantum system. For the case of $\Omega_a = 2\Gamma_0$, shown in Fig. 7(b), the situation is dramatically modified since absorption can be either enhanced up to a factor of 62 (thick solid curve) or it is reversed into gain at the sidebands. This strong dependence of the shape of

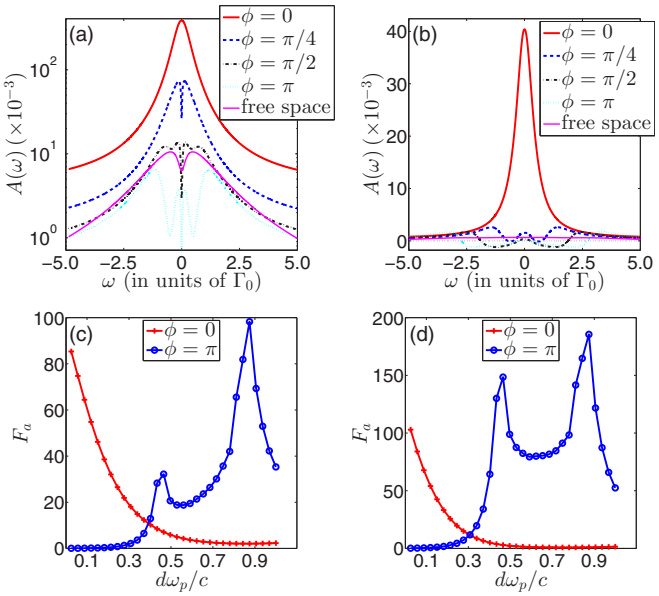

FIG. 7. Steady-state absorption spectrum $A(\omega)$ for the degenerate system ($\omega_{32} = 0$) driven on resonance $\delta = 0$ along transitions $|0\rangle \leftrightarrow |2\rangle$ and $|0\rangle \leftrightarrow |3\rangle$. The distance is $d = 0.1c/\omega_p$. A weak probe field is applied along the two transitions. The phase difference of the driving field is set to $\phi = 0$ (thick solid curve), $\phi = \pi/4$ (dashed curve), $\phi = \pi/2$ (dashed-dotted curve), and $\phi = \pi$ (dotted curve). The thin solid curve corresponds to the spectrum of the isolated quantum system. The rest of the parameters are as in Figs. 4(a) and 4(b). Lower panel: Enhancement factor of absorption at the central line F_a versus the distance for $\phi = 0$ (+) and $\phi = \pi$ (○). Rabi frequencies are $\Omega_a = 0.64\Gamma_0$ [(a) and (c)] and $\Omega_a = 2\Gamma_0$ [(b) and (d)].

the absorption spectrum on the phase ϕ is also evident for all distances between the quantum system and the plasmonic nanostructure (not shown here).

We define the enhancement factor of the absorption at the central line as $F_a = A(\omega = 0)/A_{\rm isol}(\omega = 0)$, with $A_{\rm isol}(\omega = 0)$ being the value of the absorption at $\omega = 0$ for the isolated quantum system. In order to investigate more thoroughly the strong dependence of absorption on ϕ and Ω_a, we have calculated F_a [in Figs. 7(c) and 7(d)] for all the distances considered so far and for the two previously considered Rabi frequencies. For $\phi = 0$ we obtain a monotonic decrease of F_a as the distance increases, for the two Rabi frequencies considered. For $\phi = \pi$ the maximum value of F_a is obtained for $d = 0.9c/\omega_p$, wherein a hundredfold enhancement is achieved.

In summary, the level of absorption or gain of the hybrid nanostructure can be tailored by a proper choice of the distance of the quantum system from the nanostructure, the Rabi frequencies of the pump fields, and their relative phase.

IV. CONCLUSIONS

In this work we have presented a theoretical analysis of the absorption spectrum of a four-level double-V-type quantum system in close proximity to a plasmonic nanostructure in the weak-coupling regime. One of the V-type subsystems is strongly influenced by the localized surface plasmons of the nanostructure while the other one interacts with ordinary vacuum. The plasmonic nanostructure considered is a two-dimensional array of metal-coated dielectric nanospheres. We consider different coupling configurations of the quantum system by the pump and probe laser fields. The nanostructure introduces a strongly anisotropic coupling among the decay rates of the optical transitions which modifies dramatically the absorption of a weak probe in every coupling scenario. In the case of pumping one optical transition and applying the probe field to the adjacent transition, we predict a huge enhancement of the absorption at the central line. When the probe field is applied along the same channel as the pump field it is shown that gain without inversion can be obtained. Finally, when both transitions are pumped and probed we show that a huge enhancement of absorption can be obtained compared to the free-space case. Finally, we have shown that the enhancement of absorption or gain can be controlled through different external parameters: the distance of the quantum system from the plasmonic nanostructure, the intensity of the pump field(s) and, when applicable, their relative phase.

ACKNOWLEDGMENTS

F.C. and M.A.R. acknowledge support by MICINN (Spain) through Project No. FIS2013-41709-P. F.C. also acknowledges funding from MECD through Grant No. PRX16/00473. E.P. acknowledges the support of "Research Projects for Excellence IKY/Siemens" (Contract No. 23343).

APPENDIX: ABSORPTION SPECTRUM OF A WEAK PROBE FIELD

Projecting Eq. (14) on both sides along the different states allows one to derive the time evolution of the density matrix elements, which reads

$$\dot{\rho}_{00}(t) = 2\gamma'[\rho_{22}(t) + \rho_{33}(t)] + 2\gamma''\rho_{11}(t) - i\frac{\Omega_a}{2}[\rho_{02}(t)e^{-i\phi} - \rho_{20}(t)e^{i\phi}] - i\frac{\Omega_b}{2}[\rho_{03}(t) - \rho_{30}(t)], \tag{A1}$$

$$\dot{\rho}_{22}(t) = -2(\gamma + \gamma')\rho_{22}(t) + i\frac{\Omega_a}{2}[\rho_{02}(t)e^{-i\phi} - \rho_{20}(t)e^{i\phi}] - \kappa[\rho_{23}(t) + \rho_{32}(t)], \tag{A2}$$

$$\dot{\rho}_{33}(t) = -2(\gamma + \gamma')\rho_{33}(t) + i\frac{\Omega_b}{2}[\rho_{03}(t) - \rho_{30}(t)] - \kappa[\rho_{23}(t) + \rho_{32}(t)], \tag{A3}$$

$$\dot{\rho}_{01}(t) = -\gamma''\rho_{01}(t) + i\frac{\Omega_a}{2}e^{i\phi}\rho_{21}(t) + i\frac{\Omega_b}{2}\rho_{31}(t), \tag{A4}$$

$$\dot{\rho}_{21}(t) = (i\delta - \gamma - \gamma' - \gamma'')\rho_{21}(t) - \kappa\rho_{31}(t) + i\frac{\Omega_a}{2}e^{-i\phi}\rho_{01}(t), \tag{A5}$$

$$\dot{\rho}_{31}(t) = (i\delta - \gamma - \gamma' - \gamma'')\rho_{31}(t) - \kappa\rho_{21}(t) + i\frac{\Omega_b}{2}\rho_{01}(t), \tag{A6}$$

$$\dot{\rho}_{20}(t) = (i\delta - \gamma - \gamma')\rho_{20}(t) + i\frac{\Omega_a}{2}e^{-i\phi}[\rho_{00}(t) - \rho_{22}(t)] - i\frac{\Omega_b}{2}\rho_{23}(t) - \kappa\rho_{30}(t)\,, \tag{A7}$$

$$\dot{\rho}_{30}(t) = (i\delta - \gamma - \gamma')\rho_{30}(t) + i\frac{\Omega_b}{2}[\rho_{00}(t) - \rho_{33}(t)] - i\frac{\Omega_a}{2}e^{-i\phi}\rho_{32}(t) - \kappa\rho_{20}(t)\,, \tag{A8}$$

$$\dot{\rho}_{23}(t) = (-2\gamma - 2\gamma')\rho_{23}(t) + i\frac{\Omega_a}{2}e^{-i\phi}\rho_{03}(t) - i\frac{\Omega_b}{2}\rho_{20}(t) - \kappa[\rho_{22}(t) + \rho_{33}(t)]\,, \tag{A9}$$

where $\rho_{00}(t) + \rho_{11}(t) + \rho_{22}(t) + \rho_{33}(t) = 1$ has been assumed, and $\rho_{nm}(t) = \rho^*_{mn}(t)$.

We now proceed to the calculation of the probe absorption spectrum for our system. We define the following vector,

$$U(t) = [\rho_{11}(t), \rho_{22}(t), \rho_{33}(t), \rho_{30}(t), \rho_{03}(t), \rho_{20}(t), \rho_{02}(t), \rho_{32}(t), \rho_{23}(t)]^T\,, \tag{A10}$$

where T stands for transpose, and write the equations of the density matrix in a matrix form as

$$\frac{d}{dt}U(t) = MU(t) + B\,, \tag{A11}$$

where M is a (9×9) matrix and B is a column vector whose coefficients can be determined from the density matrix equations. Steady-state values for populations and coherences are derived through $U(\infty) = M^{-1}(-B)$.

To determine the absorption spectrum in the bare-state basis we make use of vector $U(t)$ defined in Eq. (A10). The evaluation of the two-time correlation functions that appear in Eq. (24) can be recast to

$$A(\omega) \propto |\mu'|^2\,\mathrm{Re}\left[\int_0^\infty \{[\langle\sigma_{03}(\tau)\sigma_{30}(0)\rangle - \langle\sigma_{30}(0)\sigma_{03}(\tau)\rangle] + [\langle\sigma_{02}(\tau)\sigma_{20}(0)\rangle - \langle\sigma_{20}(0)\sigma_{02}(\tau)\rangle]\}e^{-i\omega\tau}d\tau\right]. \tag{A12}$$

Equation (A12) can be written as $A(\omega) = A_{03}(\omega) + A_{02}(\omega)$:

$$A_{03}(\omega) \propto |\mu'|^2\,\mathrm{Re}\left[\int_0^\infty [\langle\sigma_{03}(\tau)\sigma_{30}(0)\rangle - \langle\sigma_{30}(0)\sigma_{03}(\tau)\rangle]e^{-i\omega\tau}d\tau\right],$$

$$A_{02}(\omega) \propto |\mu'|^2\mathrm{Re}\left[\int_0^\infty [\langle\sigma_{02}(\tau)\sigma_{20}(0)\rangle - \langle\sigma_{20}(0)\sigma_{02}(\tau)\rangle]\,e^{-i\omega\tau}d\tau\right]. \tag{A13}$$

$A_{03}(\omega)[A_{02}(\omega)]$ is the absorption produced along the transition $|0\rangle \leftrightarrow |3\rangle[|0\rangle \leftrightarrow |2\rangle]$. In writing Eq. (A13) we assumed that the photons produced along the two transitions do not interfere since these channels interact with a vacuum reservoir and have orthogonal dipole matrix elements.

The two-time correlation functions which appear in Eq. (A13) can be determined using the quantum regression theorem [53,54] and Eq. (A11). To this end we define the column vectors

$$\hat{U}_{0j}(\tau) = [\langle\sigma_{11}(\tau)\sigma_{0j}(0)\rangle, \langle\sigma_{22}(\tau)\sigma_{0j}(0)\rangle, \langle\sigma_{33}(\tau)\sigma_{0j}(0)\rangle, \langle\sigma_{03}(\tau)\sigma_{0j}(0)\rangle, \langle\sigma_{30}(\tau)\sigma_{0j}(0)\rangle, \langle\sigma_{02}(\tau)\sigma_{0j}(0)\rangle, \langle\sigma_{20}(\tau)\sigma_{0j}(0)\rangle, \langle\sigma_{23}(\tau)\sigma_{0j}(0)\rangle, \langle\sigma_{32}(\tau)\sigma_{0j}(0)\rangle]^T\,, \quad (j = 3,2)\,, \tag{A14}$$

$$\hat{U}_{j0}(\tau) = [\langle\sigma_{0j}(0)\sigma_{11}(\tau)\rangle, \langle\sigma_{0j}(0)\sigma_{22}(\tau)\rangle, \langle\sigma_{0j}(0)\sigma_{33}(\tau)\rangle, \langle\sigma_{0j}(0)\sigma_{03}(\tau)\rangle, \langle\sigma_{0j}(0)\sigma_{30}(\tau)\rangle, \langle\sigma_{0j}(0)\sigma_{02}(\tau)\rangle, \langle\sigma_{0j}(0)\sigma_{20}(\tau)\rangle, \langle\sigma_{0j}(0)\sigma_{23}(\tau)\rangle, \langle\sigma_{0j}(0)\sigma_{32}(\tau)\rangle]^T\,, \quad (j = 3,2)\,, \tag{A15}$$

where the superindex T stands for transpose. According to the quantum regression theorem, for $\tau > 0$ the vectors $\hat{U}_{0j}$ and $\hat{U}_{j0}$ satisfy

$$\frac{d\,\hat{U}_{0j}(\tau)}{d\tau} = M\hat{U}_{0j}(\tau) + B\langle\sigma_{0j}(\infty)\rangle\,,$$
$$\frac{d\,\hat{U}_{j0}(\tau)}{d\tau} = M\hat{U}_{j0}(\tau) + B\langle\sigma_{0j}(\infty)\rangle\,, \tag{A16}$$

with M being the 9×9 matrix of the coefficients of Eq. (A11) and B the corresponding column vector.

By working in the Laplace space we obtain the steady-state absorption spectrum. Specifically, we have

$$A(\omega) \propto \Gamma_0\mathrm{Re}\left\{\sum_{l=1}^{l=9} R_{4,l}(iz)\big(\hat{U}^{(l)}_{03}(0) - \hat{U}^{(l)}_{30}(0)\big) + \sum_{l=1}^{l=9} R_{6,l}(iz)\big(\hat{U}^{(l)}_{02}(0) - \hat{U}^{(l)}_{20}(0)\big)\right\}, \tag{A17}$$

where $\hat{U}^{(l)}_{0j}(0)[\hat{U}^{(l)}_{j0}(0)]$ is the value of the lth component of the vector $\hat{U}_{0j}(\tau)[\hat{U}_{j0}(\tau)]$ evaluated at $\tau = 0$. $R_{jk}(iz)$ is the (j,k) element of the matrix $R(iz)$, defined as

$$R(iz) = (iz\hat{I} - M)^{-1}, \tag{A18}$$

with $\hat{I}$ being the identity matrix with size 9×9, and $z = (\omega_p - \omega_L)/\Gamma_0$.

[1] W. Zhang, A. O. Govorov, and G. W. Bryant, Phys. Rev. Lett. **97**, 146804 (2006).

[2] R. D. Artuso and G. W. Bryant, Phys. Rev. B **82**, 195419 (2010).

[3] A. Hatef, D. G. Schindel, and M. R. Singh, Appl. Phys. Lett. **99**, 181106 (2011).
[4] S. G. Kosionis, A. F. Terzis, V. Yannopapas, and E. Paspalakis, J. Phys. Chem. C **116**, 23663 (2012).
[5] S. M. Sadeghi, Phys. Rev. B **79**, 233309 (2009).
[6] S. M. Sadeghi, Phys. Rev. B **82**, 035413 (2010).
[7] M. A. Antón, F. Carreño, S. Melle, O. G. Calderón, E. Cabrera-Granado, J. Cox, and M. R. Singh, Phys. Rev. B **86**, 155305 (2012).
[8] A. Hatef, S. M. Sadeghi, and M. R. Singh, Nanotechnology **23**, 205203 (2012).
[9] M. A. Antón, F. Carreño, S. Melle, O. G. Calderón, E. Cabrera-Granado, and M. R. Singh, Phys. Rev. B **87**, 195303 (2013).
[10] E. Paspalakis, S. Evangelou, and A. F. Terzis, Phys. Rev. B **87**, 235302 (2013).
[11] W.-X. Yang, A.-X. Chen, Z. Huang, and R.-K. Lee, Opt. Express **23**, 13032 (2015).
[12] S. M. Sadeghi, Nanotechnology **21**, 455401 (2010).
[13] S. G. Kosionis, A. F. Terzis, S. M. Sadeghi, and E. Paspalakis, J. Phys.: Condens. Matter **25**, 045304 (2013).
[14] S. M. Sadeghi, Phys. Rev. A **88**, 013831 (2013).
[15] D.-X. Zhao, Y. Gu, J. Wu, J.-X. Zhang, T.-C. Zhang, B. D. Gerardot, and Q.-H. Gong, Phys. Rev. B **89**, 245433 (2014).
[16] K. E. Dorfman, P. K. Jha, D. V. Voronine, P. Genevet, F. Capasso, and M. O. Scully, Phys. Rev. Lett. **111**, 043601 (2013).
[17] A. V. Malyshev and V. A. Malyshev, Phys. Rev. B **84**, 035314 (2011).
[18] B. S. Nugroho, A. A. Iskandar, V. A. Malyshev, and J. Knoester, J. Chem. Phys. **139**, 014303 (2013).
[19] B. S. Nugroho, V. A. Malyshev, and J. Knoester, Phys. Rev. B **92**, 165432 (2015).
[20] S. H. Asadpour and H. R. Soleimani, J. Appl. Phys. **119**, 023102 (2016).
[21] J.-B. Li, N.-C. Kim, M.-T. Cheng, L. Zhou, Z.-H. Hao, and Q.-Q. Wang, Opt. Express **20**, 1856 (2012).
[22] E. Paspalakis, S. Evangelou, S. G. Kosionis, and A. F. Terzis, J. Appl. Phys. **115**, 083106 (2014).
[23] J.-J. Li and K.-D. Zhu, Crit. Rev. Solid State Mater. Sci. **39**, 25 (2014).
[24] S. K. Singh, M. K. Abak, and M. E. Tasgin, Phys. Rev. B **93**, 035410 (2016).
[25] M. R. Singh, Nanotechnology **24**, 125701 (2013).
[26] D. Turkpence, G. B. Akguc, A. Bek, and M. E. Tasgin, J. Opt. (Bristol, UK) **16**, 105009 (2014).
[27] I. Thanopulos, E. Paspalakis, and V. Yannopapas, Phys. Rev. B **85**, 035111 (2012).
[28] S. Evangelou, V. Yannopapas, and E. Paspalakis, Phys. Rev. A **86**, 053811 (2012).
[29] L. Wang, Y. Gu, H. Chen, J.-Y. Zhang, Y. Cui, B. D. Gerardot, and Q.-H. Gong, Sci. Rep. **3**, 2879 (2013).
[30] E. Paspalakis, S. Evangelou, V. Yannopapas, and A. F. Terzis, Phys. Rev. A **88**, 053832 (2013).
[31] S. Evangelou, V. Yannopapas, and E. Paspalakis, J. Mod. Opt. **61**, 1458 (2014).
[32] H. Chen, J. Ren, Y. Gu, D.-X. Zhao, J. Zhang, and Q. Gong, Sci. Rep. **5**, 18315 (2015).
[33] A. F. Terzis, S. G. Kosionis, J. Boviatsis, and E. Paspalakis, J. Mod. Opt. **63**, 451 (2016).
[34] J. Ren, H. Chen, Y. Gu, D.-X. Zhao, H. Zhou, J. Zhang, and Q. Gong, Nanotechnology **27**, 425205 (2016).
[35] M. Jabbari, Physica B: Condens. Matter **488**, 13 (2016).
[36] S. Evangelou, V. Yannopapas, and E. Paspalakis, Phys. Rev. A **83**, 023819 (2011).
[37] H. T. Dung, L. Knoll, and D. G. Welsch, Phys. Rev. A **66**, 063810 (2002).
[38] A. González-Tudela, P. A. Huidobro, L. Martín-Moreno, C. Tejedor, and F. J. García-Vidal, Phys. Rev. B **89**, 041402 (2014).
[39] P. Törmä and W. L. Barnes, Rep. Prog. Phys. **78**, 013901 (2015).
[40] R. Chikkaraddy, B. Nijs, F. Benz, S. J. Barrow, O. A. Scherman, E. Rosta, A. Demetriadou, P. Fox, O. Hess, and J. J. Baumberg, Nature (London) **535**, 127 (2016).
[41] I. Thanopulos, V. Yannopapas, and E. Paspalakis, Phys. Rev. B **95**, 075412 (2017).
[42] G. X. Li, F.-L. Li, and S.-Y. Zhu, Phys. Rev. A **64**, 013819 (2001).
[43] Y.-P. Yang, J.-P. Xu, H. Chen, and S.-Y. Zhu, Phys. Rev. Lett. **100**, 043601 (2008).
[44] G.-X. Li, J. Evers, and C. H. Keitel, Phys. Rev. B **80**, 045102 (2009).
[45] P. K. Jha, X. Ni, C. Wu, Y. Wang, and X. Zhang, Phys. Rev. Lett. **115**, 025501 (2015).
[46] G. S. Agarwal, Phys. Rev. Lett. **84**, 5500 (2000).
[47] V. Yannopapas, E. Paspalakis, and N. V. Vitanov, Phys. Rev. Lett. **103**, 063602 (2009).
[48] M. Kiffner, M. Macovei, J. Evers, and C. H. Keitel, in *Progress in Optics*, edited by E. Wolf (Elsevier, Amsterdam, 2010), Vol. 55, p. 85.
[49] Y. Gu, L. Wang, P. Ren, J.-X. Zhang, T.-C. Zhang, O. J. F. Martin, and Q.-H. Gong, Nano Lett. **12**, 2488 (2012).
[50] R. Sainidou, N. Stefanou, and A. Modinos, Phys. Rev. B **69**, 064301 (2004).
[51] V. Yannopapas and N. V. Vitanov, Phys. Rev. B **75**, 115124 (2007).
[52] N. Stefanou, V. Yannopapas, and A. Modinos, Comput. Phys. Commun. **113**, 49 (1998) **132**, 189 (2000).
[53] M. O. Scully and M. S. Zubairy, *Quantum Optics* (Cambridge University Press, Cambridge, UK, 1997).
[54] M. Lax, Phys. Rev. **172**, 350 (1968).
[55] S. V. Gaponenko, *Introduction to Nanophotonics* (Cambridge University Press, Cambridge, UK, 2010).
[56] H. Lee, P. Polynkin, M. O. Scully, and S.-Y. Zhu, Phys. Rev. A **55**, 4454 (1997).
[57] G. Pirruccio, M. Ramezani, S. Rahimzadeh-Kalaleh Rodriguez, and J. G. Rivas, Phys. Rev. Lett. **116**, 103002 (2016).